Electrokinetic Potentials of Binary Self-Assembled Monolayers on Gold: Acid−Base Reactions and Double Layer Structure

Ruediger Schweiss,[†] Dieter Pleul,[†] Frank Simon,[†] Andreas Janke,[†] Petra B. Welzel,[†] Brigitte Voit,[†] Wolfgang Knoll,[‡] and Carsten Werner*[,†]

Institute of Polymer Research Dresden and The Max Bergmann Center of Biomaterials, Hohe Str. 6, D-01069 Dresden, Germany, and Max Planck Institute for Polymer Research, Ackermannweg 10, D-55128 Mainz, Germany

Received: June 18, 2003; In Final Form: November 28, 2003

The electrokinetic charge density and the dissociation behavior of the surface carboxylic acid groups in binary self-assembled monolayers (SAMs) of 11-mercaptoundecanoic acid (MUA)/11-mercapto-undecanol (MUOH), and 16-mercaptohexadecanoic acid (MHA)/hexadecanethiol (HDT) on planar gold surfaces were studied by streaming potential and streaming current measurements in aqueous electrolyte solutions. For both two-component SAMs, the isoelectric point decreased with lower surface fractions (<0.25) of the carboxy-terminated alkanethiols, indicating that electrostatic interactions of the acid anions cause the significantly attenuated acidity of high coverage COOH-terminated SAMs. This agrees well with theoretical considerations on the influence of electrostatic energy on the interfacial acid−base equilibrium. Diffuse layer charge densities calculated from zeta potentials in monovalent electrolyte solutions show that the countercharge in the diffuse layer increases with decreasing surface charge but is due to inner layer counterion adsorption still significantly lower than predicted by the standard Gouy−Chapman theory. In the case of bivalent counterions, ion binding models successfully describe the observed electrokinetic potentials.

1. Introduction

There is ongoing interest in electrostatic interactions at self-assembled monolayer (SAM) surfaces presenting ionizable groups to the liquid phase. Beyond the feasability of these model surfaces for fundamental studies on interfacial forces and double layer interactions,[1−3] they are widely used for controlling electrostatic interactions in an aqueous environment, which is essential for nucleation and (bio)mineralization,[4−7] layer-by-layer deposition of polyelectrolyte multilayers,[8,9] aggregation of charged particles,[10,11] or for liquid-crystal alignment.[12] Therefore, insights into their surface charging processes are indispensable for electrostatic switching of their surface properties in contact with salt solutions. There are numerous reports on the acid−base equilibria of the functional groups of self-assembled monolayers using force microscopies,[13−20] electrochemical techniques,[21−24] contact angle measurements,[25] or surface mass titrations.[26−28] However, no complete picture on these phenomena is established to date. Although all these studies univocally report on a significantly attenuated acidity/basicity of the functional units in a densely packed monolayer (which is often referred to as pK-shift) as compared to solution dispersed molecules, the magnitude of the shift as well as the behavior of the acid/base-functionalized monolayer upon dilution of the charge-determining molecules with a second uncharged component are sometimes even opposite and further seem to depend on the method and the monolayers used. For example, the pH at which a pure carboxy terminated monolayer is half ionized was reported in the broad range of 5.5 and 8.5 in different studies. Effects of electrostatic in-plane interactions, a reduced ion hydration due to solvent structuring near the interface and hydrogen bonding between the uncharged ionizable moieties were suggested to cause the reduced acidity/basicity. To unravel these phenomena, we systematically studied two different binary self-assembled films by coassembly of a carboxy-modified alkanthiol with a second component which has no intrinsic charge. Therefore, the surface coverage with ionizable functional groups can be reduced within an either polar (MUOH) or nonpolar (HDT) environment. Binary mixtures of 11-mercaptoundecanoic acid (MUA) and 11-mercaptoundecanol (MUOH) are hydrophilic in their wetting characteristics for all surface compositions, whereas for mixtures of 16-mercapto-hexadecanoic acid (MHA) and hexadecanethiol (HDT), the surface tension is assumed to scale linearly with the molecular composition of the surface. As revealed in Figure 1, these two systems adequately adress all the aforementioned aspects (surface coverage of dissociating sites, hydrophobicity, hydrogen bonding) which might influence the interfacial acid−base equilibria. As key tool to study the surface charging of these monolayers we applied streaming potential and streaming current measurements in rectangular microchannels consisting of two planar sample surfaces using the microslit electrokinetic setup (MES).[29,30] This technique is especially advantageous because the use of the ideal planar sample arrangement eliminates effects of surface curvature and a possible perturbation of the charge distribution which might occur with other techniques. Moreover, this method exclusively probes electrical charges at the surface and is successful in analyzing both dissociation of surface functional groups[31,32] and preferential adsorption of ions from the liquid phase.[30] The obtained electrokinetic potential (zeta potential, ζ) can then be used for the evaluation of the double layer structure.

* Corresponding author. Fax: (++49) 4658 533. E-mail werner@ipfdd.de.
[†] Institute of Polymer Research Dresden and The Max Bergmann Center of Biomaterials.
[‡] Max Planck Institute for Polymer Research.

10.1021/jp035724m CCC: $27.50
Published on Web 02/05/2004

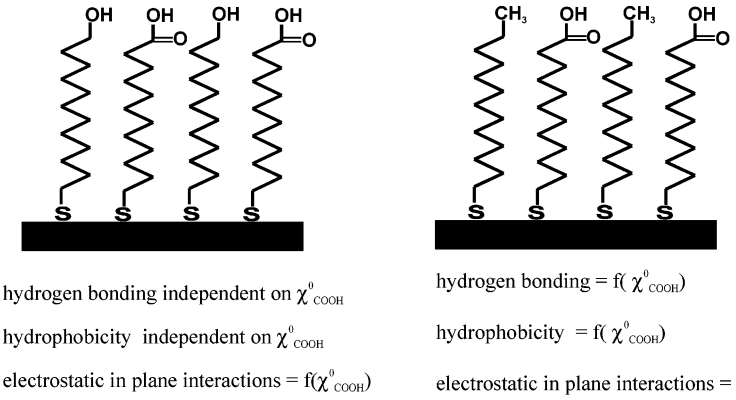

Figure 1. Expected dependency of surface properties and interactions on the surface fraction of COOH-terminated alkanethiol (χ^0_{COOH}) in self-assembled monolayers of alkanethiols on gold investigated in this study: 11-mercaptoundecanoic acid (MUA)/11-mercaptoundecanol (MUOH) and 16-mercaptohexadecanoic acid (MHA)/hexadecanethiol (HDT).

2. Background

Surface Charge at Monomolecular Films. For a binary self-assembled monolayer on gold with terminal carboxy units, the surface charge density is exclusively given by the surface concentration of carboxylate groups $\{COO^-\}_0$ provided that the second component in the monolayer does not give a significant contribution to the interfacial charge. The surface charge density (σ_0) is then given by

$$\sigma_0 = -F\{COO^-\}_0 = -F\alpha\Gamma_m\chi^0_{COOH} = -F\Gamma_m\chi^0_{COOH}\frac{\{COO^-\}_0}{\{COO^-\}_0 + \{COOH\}_0} \quad (1)$$

where Γ_m is the surface coverage of the monolayer, χ^0_{COOH} the surface fraction of COOH-terminated thiol, α the degree of dissociation and $\{COOH\}_0$ and $\{COO^-\}_0$ the surface concentrations of the protonated and the dissociated COOH groups, respectively. For high coverage alkanethiol monolayers, Γ_m is usually assumed to be 7.7×10^{-10} mol per cm^2 (1 molecule per 21.5 square Ångstroms) as revealed in helium[33] and electron diffraction studies.[34] Considering the acid−base reaction of COOH groups at the solid liquid (s−l) interface

$$-COOH(s) \rightleftarrows -COO^-(s) + H^+(l)$$

one can define the surface pK value (pK^0) as the pH of the bulk solution where half of the surface carboxy groups are dissociated:

$$pK^0 = pH + \log\frac{\{COO^-\}_0}{\{COOH\}_0} \quad (2)$$

similarly to the bulk pK value (pK^b) of solution dispersed carboxylic acids:

$$pK^b = pH + \log\frac{[COO^-]}{[COOH]} \quad (3)$$

The surface charge of such a monomolecular film is thus given by combining eqs 1 and 2

$$\sigma_0 = -\frac{F\Gamma_m\chi^0_{COOH}}{1 + pK^0 - pH} \quad (4)$$

The task is now to derive a relationship between the surface pK value (pK^0) and the bulk pK of the carboxylic acid (pK^b). Assuming a Boltzmann distribution of the protons at the interface, the latter can be related to the pH of the bulk solution

$$\{H^+\}_0 = 10^{-pH}\exp\left[-\frac{e\psi_0}{k_BT}\right] \quad (5)$$

where e is the elementary charge, k_B the Boltzmann constant, and ψ_0 the potential of the plane of the COOH groups (or surface potential). This yields an algebraic expression for the surface charge density related to the surface potential (ψ_0) and the bulk pK value pK^b:[35,36]

$$\sigma_0 = -\frac{F\Gamma_m\chi^0_{COOH}}{1 + pK^b - pH + \frac{e\psi_0}{2.303\cdot k_BT}} = -\frac{F\Gamma_m\chi^0_{COOH}}{1 + pK^b - pH + \frac{y_0}{2.303}} \quad (6)$$

This equation is commonly known as the one-site dissociation model[35] and states that the surface pK value (pK^0) is identical to the bulk pK (pK^b) and not affected by the surface confinement of the acidic molecules but rather the acid−base equilibrium is shifted in favor of the nondissociated COOH groups resulting from a depletion of protons at the surface by a factor of the reduced surface potential y_0. Stated otherwise, the surface pK (pK^0) according to our definition in eq 2 is represented by

$$pK^0 = pK^b + \frac{y_0}{2.303}$$

If the local potential of the surface plane of the COOH groups is known, the in-plane electrostatic effect on the acid−base behavior can be calculated.

Electrokinetic Potential. The electrokinetic potential (or zeta potential ζ) describes the potential at the shear plane of the hydrodynamically fixed and mobile part of the electric double layer. For smooth surfaces that are not permeable to the solvent, ζ is a good approximation of the potential of the outer Helmholtz plane (OHP) in the Gouy−Chapman−Stern−Grahame model (GCSG) of the double layer.[37] Additionally, there is experimental evidence that for such (hard and smooth) interfaces, ζ also is in good agreement with the diffuse layer potential calculated from force−distance measurements by the DLVO theory.[38,39] The charge density of the diffuse part of the double layer is then obtained by insertion of the zeta potential values

into the Grahame equation (eq 7) and solving with respect to the parameters of the electrolyte solution (N, c_i, z_i).

$$\sigma_d = \sqrt{2k_B T \epsilon_0 \epsilon_r \sum_{i=1}^{N} c_i \left\{ \exp\left[-\frac{z_i e \xi}{k_B T} \right] - 1 \right\}} \qquad (7)$$

where z_i are the valence, c_i the bulk concentration, and N the total number of the ions in the liquid phase. As the whole double layer is electrically neutral, the surface charge in the GCSG model is compensated in (i) the Stern layer which contains solvent molecules and electrostatically fixed counterions and (ii) the diffuse layer

$$\sigma_0 = -(\sigma_{Stern} + \sigma_d) \qquad (8)$$

Binary Self-Assembled Monolayers on Gold. There is a body of work in the literature on binary self-assembled monolayers with alkanethiols of different chain lengths. When coadsorbed from two-component solution, the monolayers exhibit increasing tendency toward phase separation on the mesoscopic scale with increasing difference in chain lengths, regardless of their terminating groups.[40−42] This is because the van der Waals interactions among the hydrocarbon chains overcompensate the entropy of mixing the more the components differ in their number of methylene units. Recent molecular dynamics simulations report on a threshold value of the chain length difference of 3 methylene units.[43] If the hydrocarbon backbones are of equal chain length, most studies including reductive desorption,[44,45] wetting,[42] or friction force microscopy[46] suggest rather perfect mixing despite differences in the polarity of the terminating groups. However, it is important to note that high-resolution STM investigations[47,48] have found nanoscale domains for certain systems (mixed SAMs with $-CH_3$ and $-OCH_3$ endgroups, C16 backbone). Stated otherwise, phase separation on the molecular level might occur even when the alkane chain lengths of both components are equal.

3. Experimental Section

Monolayer Preparation. 11-Mercaptoundecanol (MUOH), 11-mercaptoundecanoic acid (MUA), and 16-mercaptohexadecanoic acid (MHA) were supplied from Aldrich (Deisenhofen, Germany), and hexadecanethiol (HDT) was obtained from Merck (Darmstadt, Germany). Polished float glass slides (length (L) 20 mm, width (b) 10 mm, Berliner Glas GmbH, Germany) were cleaned and primed with a 2 nm chromium layer to promote adhesion of gold on these carriers. Then, a 150 nm gold layer was evaporated onto the substrates at $(1-2) \times 10^{-5}$ mbar yielding gold substrates with a typical roughness 1.5−1.8 nm (rms). Prior to monolayer deposition the gold substrates were subsequently cleaned with a "snow-jet" (flushing the slightly heated surface with a stream of CO_2/dry ice) and etched in "Caro's acid" (1 g potassium peroxodisulfate in 50 mL 96% H_2SO_4), and rinsed copiously with deionized water and finally with absolute ethanol. Monolayers were deposited from alkanethiol solutions in absolute ethanol (MUA, MHA, HDT, and mixtures of MUA/MUOH) and dry THF (mixtures of MHA/HDT). Alkanethiol stock solutions of 1 mM were mixed in the desired ratio and diluted to obtain a total alkanethiol concentration of the deposition solution of 0.25 mM. After assembly, the substrates were rinsed thoroughly with absolute ethanol and dried under vacuum.

Monolayer Characterization. To control monolayer quality, the samples were examined by wetting measurements, ellipsometry and reflection-adsorption (RAIR)-FTIR spectroscopy, X-ray-photoelectron spectroscopy (XPS), and atomic force microscopy (AFM). Contact angles were measured with a Krüss DSA system (Krüss GmbH, Hamburg, Germany). The thickness of the films was determined by a submonolayer ellipsometer (Dr. Riss Ellipsometerbau, Ratzeburg, Germany). Reflection-adsorption-FTIR spectra were recorded by means of a Perkin-Elmer 1760X FTIR spectrometer (Norwalk, VA) with p-polarized light and an angle of incidence $\alpha = 82°$. Surface analysis with X-ray-photoelectron spectroscopy was performed with an AXIS ULTRA (Kratos Analytical, UK) spectrometer using monochromated Al−Kα radiation at takeoff angles of 0° and 75° (here the takeoff angle is defined as the angle between the sample surface normale and the electronoptical axis of the spectrometer). To determine the monolayer composition in the case of MUA/MUOH mixtures, the hydroxy groups were derivatized by esterification with trifluoroacetic anhydride (TFAA) according to Bertilsson et al.[49] and Hutt et al.[50] Based on this procedure, the surface fraction of OH-terminated alkanethiol can be estimated by analyzing the F 1s signals. AFM measurements were performed with a Bioscope (Digital Instruments, Santa Barbara, CA). Hydrophilic AFM tips were prepared by evaporating 20 nm gold onto silicon AFM tips and subsequently assembling MUOH onto these tips as reported above.

For MHA/HDT monolayers, the surface composition was calculated via the O/S ratio of the X-ray photoelectron spectra. MUA/MUOH monolayers were derivatized with trifluoroacetic anhydride (TFAA), which exclusively reacts with the OH groups of MUOH in the frame of the reaction time applied in this work (30 min). This is supported by the fact, that no fluorine signals were obtained for pure MUA in our measurements. Therefore it is possible to calculate the surface composition by integration of the F 1s peak in the XPS spectra. For both mixed monolayers the surface composition reflects the mole fractions in the deposition solution within an accuracy of ±0.03 (units of surface fraction). Good agreement between the composition of the liquid phase and the monolayer obtained for mixtures of SAMs with polar and nonpolar endgroups (MHA/HDT) when THF is used as a solvent was already reported by Ulman et al.[51] for mixtures of dodecanethiol and 11-mercaptoundecanol. This is also confirmed by the vibrational spectra of MHA/HDT (Figure 2 A). The infrared spectrum of MHA reveals frequencies of the methylene bands similar to HDT. Therefore, we conclude that high coverage MHA-SAMs were prepared. However, for the mixture with about 75% of MHA, the methylene vibrations slighty shift by about 4 cm^{-1} to higher wavenumbers, which indicates lower degrees of crystallinity than for the pure MHA or HDT SAMs. Likewise, wetting measurements (Figure 2B) suggest that the contact angles also reflect the surface composition, and a Cassie-like dependency of the contact angle is obtained for MHA/HDT binary monolayers. This might be seen as an additional indication that there is no phase separation of the two components on the scale of a contact angle experiment (∼1 μm). MUA/MUOH monolayers are pronouncedly hydrophilic for all surface composition. Tapping mode AFM experiments (Figure 2C) using hydrophilic tips (gold covered Si-AFM tips which were modified with MUOH) on MHA/HDT-SAMs (composition 0.47/0.53, Figure 2C right) prepared by cosorption did not show any significant domains as compared to artificially phase-separated MHA/HDT SAMs (Figure 2C left, microcontact-printed HDT-structures were "filled" by solution deposition of MHA onto the printed substrates). Therefore, we may conclude that phase separation might occur on a molecular level if at all.

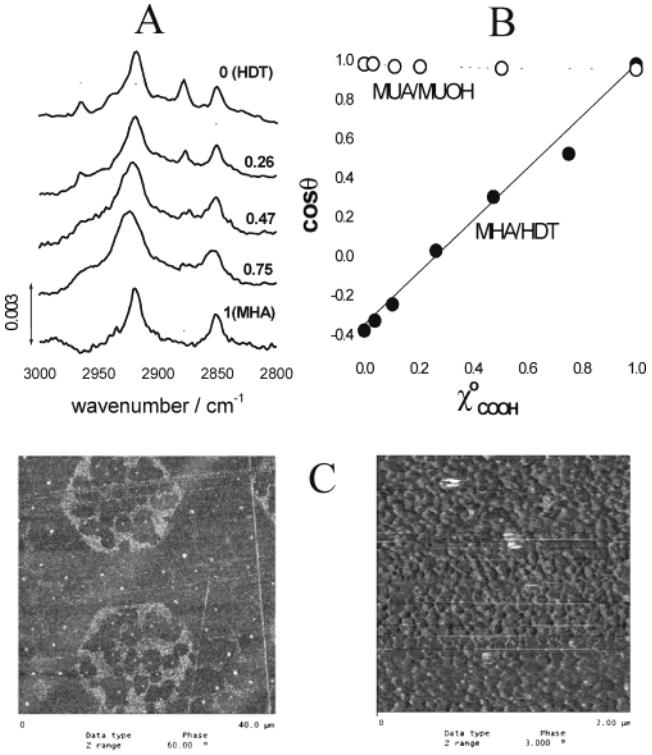

Figure 2. Ex situ characterization of binary SAMs studied in this work. (A) Reflection−absorption infrared (RAIR) spectra of selected MHA/HDT SAMs as a function of the surface composition. (B) Advancing contact angles of MHA/HDT and MUA/MUOH SAMs as a function of the surface composition. (C) Tapping mode AFM picture (phase) with a MUOH-modified Au/Si tip of gold surfaces with microcontact-printed HDT (20 μm) and gaps filled with MHA (area 40 × 40 μm, left) and a binary MHA/HDT SAM (0.47/0.53) prepared by chemisorption from THF solutions (area 2 × 2 μm, right) on gold surfaces.

Electrokinetic Measurements. The microslit electrokinetic setup (MES)[29,30] was developed for determination of the streaming potential and the streaming current of planar interfaces and enables electrokinetic experiments with excellently defined geometry. Two sample surfaces are aligned in parallel to form a rectangular microchannel. The liquid flow proceeds between two containers passing this microslit and sensors for the measurement of pH, conductivity, and temperature. Streaming potential and streaming current were recorded with a high ohmic resistance electrometer using Ag/AgCl electrodes installed at both ends of the streaming channel. All electrolyte solutions were prepared using deionized, thoroughly degassed water (Milli-Q, resistivity 18 MΩ cm^{-1}) and by means of titrators equipped with standard electrolyte solutions (KCl, HCl, KOH). The solution pH was adjusted by addition of hydrochloric acid or potassium hydroxide. Nitrogen 5.0 served as process gas to generate liquid flow in all experiments. This prevents carbon dioxide uptake from the atmosphere and thus maintains constant ionic strength and pH over long periods of time. The gas pressure was controlled by means of a pressure sensor. Measurement procedure, data collection and processing were performed with a software package written in Testpoint (Keithley Instruments). The whole setup was assembled under a laminar flow box. Further technical details of the microslit electrokinetic setup may be found in the literature.[29] The freshly prepared SAM substrates were glued to glass blocks, flushed with a stream of argon, and mounted into the microslit cell. To obtain a rectangular slit channel the samples were aligned by means of a light microscope. The height of the slit channel (h) was thoroughly adjusted by flow measurements at four different pressure differences over the channel and was set to 50 ± 0.1 μm. The streaming potential (E_S) and the streaming current (I_S) were measured by applying pressure ramps up to 200 mbar in 50 mbar steps and in both directions of the slit channel. The zeta potential (ζ) can be calculated from E_S and I_S by means of the Helmholtz−Smoluchowski equations (eqs 9 and 10) with respect to the slopes (dE_S/dp) and (dI_S/dp)

$$\zeta(E_S) = \frac{\eta}{\epsilon_0 \epsilon_r}\left[\lambda_B + \frac{2K^\sigma}{h}\right]\left(\frac{dE_S}{dp}\right) \quad (9)$$

$$\zeta(I_S) = \frac{\eta}{\epsilon_0 \epsilon_r}\frac{L}{bh}\left(\frac{dI_S}{dp}\right) \quad (10)$$

where η and ϵ are the viscosity/dielectric constant of the liquid, λ_B the bulk electrolyte conductivity, and K^σ the surface conductivity. The length L and the width b of the channel are predetermined by the geometry of the sample slides (L = 20 mm, b = 10 mm). The height of the channel (h) is given by the sample distance. As reported earlier,[31,52] a conducting metal underlayer acts as a bypass for the conduction current in a streaming potential experiment and this interferes with an exact determination of the surface conductivity K^σ. Therefore the zeta potential derived from the streaming current (eq 10) is taken as an "effective" zeta potential ζ.

4. Results

Before we present the results of the electrokinetic measurements on binary mixtures, we briefly recall the zeta potentials of the single-component SAMs, namely MUA, MHA, MUOH, and HDT.

MUA and MHA Monolayers. As reported previously,[31] MUA and MHA SAMs show a strongly attenuated acidity which becomes obvious in an isoelectric point of about pH 4.3 in KCl solutions, which is significantly higher than the IEP of polymer brushes with COOH moieties such as grafted poly(acrylic acid) (PAAc),[53] grafted polyglutamic acid (PGA),[32] or spin-coated maleic anhydride-(MA)-copolymer films.[54] The IEPs of these polymer surfaces were found in a range from pH 2−2.8. Thus, the difference of about 2 units of pH is nothing else but the manifestation of the pK shift of the terminating groups in densely packed self-assembled monolayers. This isoelectric point of 4.3 is very consistent with the onset of heavy metal ion binding to COOH-terminated SAMs,[4] the decrease of the repulsion forces between MHA surfaces,[2] and the destabilization of MUA-modified gold colloids.[55] Figure 3 shows the zeta potential of MHA as a function of pH at different ionic strength. However, in the case of the bivalent calcium as background ion, the IEP shifts toward a more acidic range of pH (3.1). This is a first evidence of the fact that the pK shift is mainly for electrostatic reasons. It is also noteworthy that the zeta potentials in KCl solutions are in good agreement with AFM surface potentials in similar monovalent electrolytes.[16−18] This underlines the consistency of electrokinetic and DLVO theory for these smooth and well-defined surfaces.

MUOH and HDT Monolayers. It is important to note that also monolayers without dissociable sites accumulate negative surface charge upon contact with aqueous electrolyte solution. Recent AFM experiments on HDT SAMs[56] or perfluorinated SAMs[57] as well as electrokinetic measurements on hydrophobic HDT[31] monolayers (and also octadecanethiol ODT and hydrophobic fluorpolymers,[30] e.g.) reveal a negative charge at pH > 4. The reversal of the surface forces and the sign of the zeta potential takes place near pH 4 being independent of the

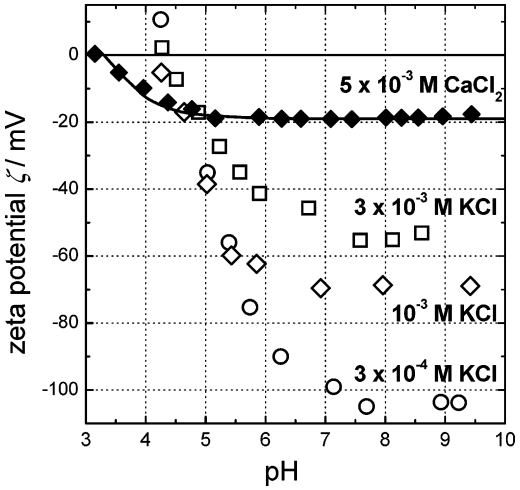

Figure 3. Electrokinetic potentials (ζ) of a MHA SAM on gold as a function of pH in different background electrolytes. The solid line represents a fit of the zeta potentials with calcium chloride as background electrolyte to the counterion condensation model (eq 14) with $pK^b = 5.15$ and $K_{Ca} = 2.55$.

background electrolyte concentration. Likewise, the zeta potential of the alkane (docosane)−water interface was found to monotonically decrease with increasing KCl concentration.[58] This means that, for these surfaces the IEP of pH 4 is equivalent to the point of zero charge (PZC). Consequently, the negative surface charge over a wide range of pH is therefore established by preferential adsorption of hydroxide ions. Recent studies and theoretical efforts on hydrophilic interfacial systems confirm the dominating role of hydroxide ions in the surface charge formation of nondissociating organic surfaces regardless of their hydrophilicity.[59] Therefore, isoelectric points of about 4 were found for insoluble monolayers of long-chain alcohols[60] and poly(ethylene glycol) ethers[61] at the air−water interface as well. Moreover, model calculations[59] as well as electrokinetic measurements (zeta potential and surface conductivity)[30] show that the surface charge densities due to preferential adsorption of ions from the solutions are limited by electrostatic repulsion of the adsorbed ions and vary in the range of about 1−1.5 μC per cm^2.[59] These values are much lower than the charge densities that are generated by dissociation of COOH-terminated SAMs. Therefore, the contribution of the diluent to the surface charging can be neglected in most cases, especially as ion adsorption on the systems used in this study should be strongly prevented by electrostatic repulsion of anions by the carboxylate groups.

MHA/HDT Monolayers. Figure 4 (top) shows the zeta potentials for selected binary monolayers from MHA and HDT. Whereas the monolayers with higher content of MHA show even higher isoelectric points, the monolayers with low surface fractions of carboxy groups (MHA) display a significant shift of the IEP toward the acidic range. At the same time the absolute values of the zeta potential increase with decreasing content of MHA. This is astonishing at first glance because the surface charge density due to ionization is also supposed to decrease when a MHA monolayer is diluted with HDT molecules.

MUA/MUOH Monolayers. Figure 4 (bottom) depicts the zeta potentials of various binary self-assembled monolayers of MUA/MUOH. For all compositions the isoelectric point of the mixtures is lower than the IEP of pure MUA (IEP = 4.3). For the monolayers with a MUA surface fraction of 0.11 an IEP of about 2.7 is obtained which is pronouncedly acidic and comparable with maleic acid copolymers, or grafted polymers with COOH groups.

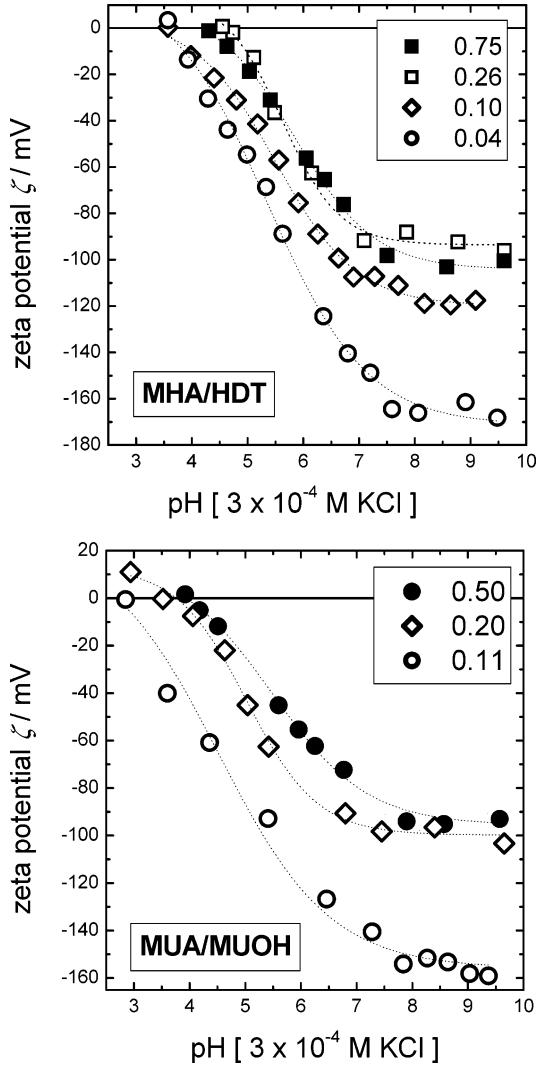

Figure 4. Electrokinetic potentials (zeta) of binary MUA/MUOH and MHA/HDT SAMs on gold as a function of the surface composition (surface fraction of COOH-terminated alkanethiol). Background electrolyte 3×10^{-4} M KCl.

TABLE 1: Isoelectric Points (IEPs) of Binary MUA/MUOH and MHA/HDT SAMs on Gold as a Function of the Surface Composition (surface fraction of COOH-terminated alkanethiol χ^0_{COOH})[a]

monolayer	surface fraction of COOH χ^0_{COOH}	isoelectric point (pH_{IEP})
MUA/MUOH	0.03	3.4
	0.11	2.7
	0.21	3.5
	0.51	3.9
	1.00	4.3
MHA/HDT	0.04	3.7
	0.10	3.4
	0.26	4.6
	0.47	4.5
	0.75	4.4
	1.00	4.3

[a] Background electrolyte 3×10^{-4} M KCl.

5. Discussion

Table 1 summarizes the isoelectric points of the two binary systems as a function of the surface composition. At lower coverages of the acidic-terminated alkanethiol (χ^0_{COOH}) both two-component monolayers exhibit an IEP that is typical of acid-

modified surfaces. Whereas for MUA/MUOH the increased acidity is observed even at lower degrees of dilution with MUOH, the hydrophobic system MHA/HDT shows an increased acidity only if the content of MHA is below a surface fraction of 0.25.

One might give an interpretation based on an effect of the hydrophobic environment of the carboxy groups which, besides the electrostatic interaction, additionally suppresses the ionization. As known from theoretical considerations and sum-frequency spectroscopy,[62] interfacial water experiences substantial ordering at hydrophobic surfaces. This ordering process is accompanied by a low permittivity and is therefore unfavorable for ion solvation. Based on this assumption one may conclude that the acidity of ionizable groups decreases if they are embedded in a hydrophobic matrix. The other idea invokes a nanoscale phase separation. That is, at higher fractions of the acidic component, the latter forms nanoscale domains which themselves behave just like the pure MHA SAM in terms of charge formation. When the content of MHA is lowered to a certain threshold value (in this case about 10−20% content of the COOH-terminated alkanthiol) there might be no interference of neighboring carboxy groups and the IEP thus shift toward the acidic range. These ideas together with the fact that the domains do not exceed the molecular level might adequately explain why the IEP of the MHA/HDT system hardly varies for COOH surface fractions of 0.25 to 1.

Contrarily, MUA/MUOH monolayers are expected to show perfect mixing of the two components. This is because the MUOH matrix has the same surface energy as a pure MUA SAM. In this case the electrostatic interactions are reduced by any dilution with the polar component.

All those observations on the binary system clearly reveal that electrostatic interactions are mainly the governing factor for the attenuated acidity of carboxy groups in a self-assembled monolayer. Effects of hydrogen bonding between the carboxylic moieties on the acid−base behavior can obviously be neglected because otherwise the MUA/MUOH system should not reveal low IEPs. At fractions of MUA and MHA below 0.05 the IEP increases again. This is reasonable because at the low content of COOH groups the surface charging process of ion adsorption becomes increasingly competitive and therefore the IEP moves toward 4.0, which is the IEP for $\chi^0_{COOH} = 0$. It is generally interesting in how far the charge density for the whole set of the mixed systems is affected by the interplay of dissociation and ion adsorption. The differences in terms of the acid−base behavior (see Figure 4) of the MHA/HDT and MUA/MUOH systems might also be related to the differences in ion affinity. In other words, ion adsorption effects are possibly underestimated for the treatment of COOH surfaces.

Focusing exclusively on electrostatic factors, recent models of Aoki et al.[63] and Borkovec[64] predict the attenuated acidity on the basis of electrostatic interactions on the molecular level instead of the reduced surface potential. Assuming a hexagonal structure of the alkanethiols,[34] every carboxy group of a pure acidic monolayer experiences the electric fields of at least six next neighboring groups at high pH. Therefore the shift of the pK is given by B[63]

$$B = \frac{3e^2}{\epsilon_0 \epsilon_r r_0}\sqrt{\alpha} \tag{11}$$

where r_0 is the minimum interdistance of the carboxy groups in the uncharged state. The mean field model[64] states the electrostatic shift B as a function of the potential of mean force $\langle E \rangle$

$$B = \frac{\langle E \rangle \sqrt{\alpha}}{2.303RT} \tag{12}$$

Both models predict a broadening and a shift of the inflection point versus the alkaline range of the titration curve. For example assuming the bulk pK value of carboxylic acids of 4.8 and a spacing of 0.5 nm per carboxy group, the pH of half-ionization resulting from eq 9 is shifted for about 1.3 units of pH, which is comparable with our variance of the isoelectric points by reducing the coverage by cosorption of a diluent. Similarly, recent studies of Sugihara et al.[28] report on a tuning of the surface coverage of alkanethiol SAMs by variation of the deposition time. Applying the quartz crystal microbalance (QCM) in situ, they observed a variation of the pK from 4.5 to 6.5 for surface coverages of 2 and 8 × 10^{-10} mol cm^{-2}, respectively. Likewise, reflectometry on poly(acryl acid) brushes of different grafting density reveals a shift of the acid−base equilibrium toward higher pH with increasing grafting density.[65]

Altogether, these findings indicate that mainly the interactions of the COOH group, presumably electrostatic ones, are responsible for the lowered acidity in SAMs and that the intrinsic pK of the COOH (considering electrostatics on the acid−base equilibrium) is very close to the bulk pK (pK^b), at least for the hydrophilic MUA/MUOH system. Beyond the influence of the surface density of ionziable groups on their acidity itself, the countercharge distribution in the double layer is similarly affected by the surface charge density. For a pure MHA monolayer, the diffuse layer charge density calculated with eq 7 is only 2% of the assumed surface charge density. This value is well in agreement with force distance measurements and electrochemical AFM.[3] For the bivalent ion Ca^{2+}, strong binding of the bivalent cations to the carboxylate groups is expected[66] and thus the electrokinetic potentials can be modeled invoking counterion condensation phenomena.[67−69] Assuming that one bivalent ion is shared by two carboxy groups, then the following reaction

$$COO^-(s) + 0.5Ca^{2+}(l) \leftrightarrow COO_{1/2}Ca(s)$$

yields a binding constant of calcium ions K_{Ca}

$$K_{Ca} = \frac{\{Ca^{2+}\}_0^{1/2}\{COO^-\}_0}{\{COOCa_{1/2}\}_0} \tag{13}$$

Assuming a Boltzmann distribution of the calcium ions, one finally obtains for the surface charge density of MHA SAM ($\chi^0_{COOH} = 1$).

$$\sigma_0 = -\frac{F\Gamma_m}{1 + \frac{[H^+]}{10^{-pK_b}}\exp\left\{-\frac{e\,\zeta}{2.303\,k_BT}\right\} + \frac{[Ca^{2+}]^{1/2}}{K_{Ca}}\exp\left\{-\frac{2e\,\zeta}{2.303\,k_BT}\right\}^{1/2}} \tag{14}$$

Solving the Grahame equation for a 2−1 electrolyte and equating with eq 14 relates the charge densities to the binding constants and the pK values. As revealed in Figure 3, the numerical fitting of the zeta potential to the model above is quite fair and yields a pK^b of 5.15 and a pK_{Ca} of 2.55. That means, that in 5 × 10^{-3} M $CaCl_2$ solutions the dissociation of the endgroups of the MHA monolayers is much less impeded

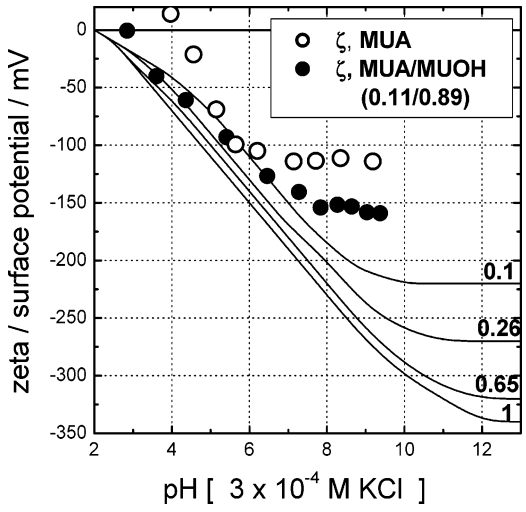

Figure 5. Comparison of the zeta potentials of pure MUA (open circles) and a MUA/MUOH SAM (0.11/0.89, solid circles) with calculated Gouy−Chapman surface potentials (eq 6) in 3×10^{-4} M KCl (assuming $\Gamma_m = 7.7 \times 10^{-10}$ mol cm^{-2} and $pK^b = 4.8$) for different surface fractions of carboxy groups (labeled numbers).

as compared to dilute KCl solutions, and the surface pK (pK^0) is consequently very close to the bulk pK^b in this case. The zeta potential of a MHA monolayer in 10^{-2} M $CaCl_2$ at pH 10 was found to be still negative (−11 mV), indicating that no charge reversal occurs at this pH. As shown in Figure 4, the zeta potentials increase in magnitude even though the surface charge density decreases with the degree of dilution. This observation is in agreement with double layer theories as they predict that the lower the surface charge the more diffuse (Gouy−Chapman-like) is the counterion distribution. Stated otherwise, with decreasing surface charge density the electrostatic forces on the counterions are weakened as well, and thus more of them are electrokinetically available. In contrast, elevated surface charge densities will cause higher degrees of charge compensation within the hydrodynamically stagnant part of the interface and, therefore, decrease the magnitude of the electrokinetic potential. For pure MUA and MHA SAMs and mixtures with about $\chi^0_{COOH} > 0.2$, only a few percent of the countercharges are located in the diffuse layer. Conversely, for example, for a MUA/MUOH (0.1/0.9) SAM the diffuse layer charge density is about 30% of the estimated surface charge density.

Numerical calculations as a function of density of carboxy groups based on a combination of the Gouy−Chapman model ($\sigma_d = -\sigma_0$) and the site-binding model (eq 6) assuming a high coverage alkanethiol monolayer (1 molecule per 21.5 square Ångstroms[34]) and a pK of 5, reveal that even for lower coverage of COOH-terminated thiols, the standard Gouy−Chapman model is inadequate and predicts higher potentials than observed by the electrokinetic measurements (Figure 5). The surface potentials would be so high that, according to the Boltzmann distribution ($|F\Psi| \gg k_BT$, eq 5), an enormous depletion of hydroxide ions at the surface would arise and the surface pH consequently would become much lower than the bulk value. Assuming a bulk p*K* value 5, only 50% of the COOH groups in the pure COOH-terminated SAMs would be ionized at pH 10, which is not in accordance with our experiments. Nevertheless, as obvious from Figure 5, the experimental results for a SAM with a low content of COOH ($\chi^0_{COOH} = 0.1$) markedly approach, especially at low pH, the curve predicted by the GC/site-binding model. This underlines the validity of the Gouy−Chapman approximation in the low surface charge density regime.

Finally, it is important to note that, consistent with the prevailing influence of electrostatic interactions, the tremendous increase in the acidity (or decrease of the isoelectric point) coincides with the steep increase of diffuse layer charge. Stated otherwise, the interfacial acid−base equilibrium and the counterion distribution are both directly related to the strength of electrostatic interactions among the carboxy moieties.

6. Summary and Conclusions

Electrokinetic measurements on planar substrates were applied to investigate the influence of ionizable surface groups in self-assembled monolayers on the acid−base behavior and the counterion distribution across the electrochemical double layer. By varying systematically the surface coverage of charge-determining groups and the surface tension of the interfacial systems it was possible to ascribe the pK shift in monomolecular films mainly to electrostatic interactions. Following these assumptions, surface fractions of carboxy groups of about 10% yielded the most "acidic" character. The lower acidity of the MHA/HDT system, as compared to the MUA/MUOH SAMs, might be due to nanoscale phase separation of the MHA/HDT mixtures.

In agreement with theoretical predictions, the calculated diffuse layer charge densities show that the counterions are increasingly distributed in a space-charge layer with decreasing surface charge density. To confirm the ideas about electrostatic interactions, additional experiments with higher ionic strength and bi-order trivalent ions or measurements on surface attached polymer brushes of different grafting density could be useful.

Acknowledgment. The authors thank Dr. Mingtai Wang (Institute of Polymer Research Dresden) for his kind assistance with the microprinted SAMs. R.S. gratefully acknowledges financial support from the Sachsisches Staatsministerium fuer Wissenschaft und Kunst, Dresden, Germany.

References and Notes

(1) Frisbie, C. D.; Rozsnyai, L. F.; Noy, A.; Wrighton, M. S.; Lieber, C. M. *Science* **1994**, *265*, 2071−2073. (b) Kokkoli, E.; Zukoski, C. F. *Langmuir* **1998**, *14*, 1189−1195. (c) Molinero, V.; Calvo, E. J. *J. Electroanal. Chem.* **1998**, *445*, 17−25. (d) Ederth, T.; Claesson, P. M.; Liedberg, B. *Langmuir* **1998**, *14*, 4782−4789.

(2) van der Vegte, E. W.; Hadziiouannou, G. *Langmuir* **1997**, *13*, 4357−4368.

(3) Hu, K.; Chai, Z.; Whitesell, J. K.; Bard, A. J. *Langmuir* **1999**, *15*, 3343−3347.

(4) Sastry, M.; Patil, V.; Mayya, K. S. *J. Phys. Chem. B* **1997**, *101*, 1167−1170.

(5) Li, J.; Liang, K. S.; Scoles, G.; Ulman, A. *Langmuir* **1995**, *11*, 4418−4427.

(6) Meldrum, F. C.; Flath, J.; Knoll, W. *Langmuir* **1997**, *13*, 2033−2049. (b) Onuma, K.; Oyane, A.; Kokubo, T.; Treboux, G.; Kanzaki, N.; Ito, A. *J. Phys. Chem. B* **2000**, *104*, 11950−11956. (c) Jiang, P.; Liu, Z. F.; Cai, S. M. *Langmuir* **2002**, *18*, 4495−4499.

(7) Han, Y.-J.; Aizenberg, J. *J. Am. Chem. Soc.* **2003**, *125*, 4032−4033.

(8) Tsukruk, V. V.; Bliznyuk, V. N.; Visser, D.; Campbell, A. L.; Bunning, T. J.; Adams, W. W. *Macromolecules* **1997**, *30*, 6615−6625. (b) Godinez, L. A.; Castro, R.; Kaifer, A. E. *Langmuir* **1996**, *12*, 5087−5092.

(9) Zhu, M.; Schneider, M.; Papastavrou, G.; Akari, S.; Möhwald, H. *Langmuir* **2001**, *17*, 6471−6476.

(10) Auer, F.; Scotti, M.; Ulman, A.; Jordan, R.; Sellergren, B.; Garno, J.; Liu, G.-Y. *Langmuir* **2000**, *16*, 7554−7557. (b) Shipway, A. N.; Lahav, M.; Willner, I. *Adv. Mater.* **2000**, *12*, 993−997.

(11) Zhang, H.; Grim, P. C. M.; Liu, D.; Vosch, T.; de Feyter, S.; Wiesler, U.-M.; Beresheim, A. J.; Müllen, K.; Haesendonk, C. V.; Vandamme, N.; de Schryer, F. C. *Langmuir* **2002**, *18*, 1801−1810.

(12) Shah, R. R.; Abbott, N. L. *J. Phys. Chem. B* **2001**, *105*, 4936−4950.

(13) Smith, D. A.; Wallwork, M. L.; Zhang, J.; Kirkham, J.; Robinson, C.; Marsh, A.; Wong, M. *J. Phys. Chem. B* **2000**, *104*, 8862−8870.
(14) van der Vegte, E. W.; Hadziouannou, G. *J. Phys. Chem. B* **1997**, *101*, 9563−9569.
(15) Zhang, H.; He, H. X.; Wang, J.; Mu, T.; Liu, Z. F. *Appl. Phys. A* **1998**, *66*, 269−271.
(16) Hu, K.; Bard, A. J. *Langmuir* **1997**, *13*, 5114−5119.
(17) Kane, V.; Mulvaney, P. *Langmuir* **1998**, *14*, 3303−3311.
(18) Kokkoli, E.; Zukoski, C. F. *Langmuir* **2000**, *16*, 6029−6036.
(19) Giesbers, M.; Kleijn, J. M.; Cohen-Stuart, M. A. *J. Colloid Interface Sci.* **2002**, *252*, 138−148.
(20) Zhang, H.; He, H. X.; Mu, T.; Liu, Z. F. *Thin Solid Films* **1998**, *327*−*329*, 778−780.
(21) Kakiuchi, T.; Iida, M.; Imabayashi, S.; Niki, K. *Langmuir* **2000**, *16*, 5397−5401.
(22) Zhao, J.; Luo, L.; Yang, X.; Wang, E.; Dong, S. *Electroanalysis* **1999**, *11*, 1108−1111.
(23) Smalley, J. F.; Chalfant, K.; Feldberg, S.; Nahir, T. M.; Bowden, E. F. *J. Phys. Chem. B* **1999**, *103*, 1676−1685.
(24) Schweiss, R.; Werner, C.; Knoll, W. *J. Electroanal. Chem.* **2003**, *540*, 145−151.
(25) Creager, S. E.; Clarke, J. E. *Langmuir* **1994**, *10*, 3675−3683.
(26) Wang, J.; Frostman, L. M.; Ward, M. D. *J. Phys. Chem.* **1992**, *96*, 5224−5228.
(27) Shimazu, K.; Teranishi, T.; Sugihara, K.; Uosaki, K.; *Chem. Lett.* **1998**, *7*, 669−670.
(28) Sugihara, K.; Teranishi, T.; Shimazu, K.; Uosaki, K. *Electrochemistry* **1999**, *67*, 1172−1174.
(29) Werner, C.; Körber, H.; Zimmermann, R.; Dukhin, S. S.; Jacobasch H. J. *J. Colloid Interface Sci*. **1998**, *208*, 329−346.
(30) Zimmermann, R.; Dukhin, S. S.; Werner, C. *J. Phys. Chem. B* **2001**, *105*, 8544−8549.
(31) Schweiss, R.; Welzel, P. B.; Werner, C.; Knoll, W. *Langmuir* **2001**, *17*, 4304−4311.
(32) Werner, C.; Zimmermann, R.; Kratzmüller, T. *Colloids Surf. A* **2001**, *192*, 205−213.
(33) Chidsey, C. E. D.; Liu, G. Y.; Rowntree, Y. P.; Scoles G. *J. Chem. Phys*. **1989**, *91*, 4421−4423. (b) Ulman, A. *Chem. Rev*. **1996**, *96*, 1533−1554.
(34) Bain, C. D.; Evall, J.; Whitesides, G. M. *J. Am. Chem. Soc*. **1989**, *111*, 7155−7164.
(35) Healy, T. W.; White, L. R. *Adv. Coll. Interface Sci.* **1978**, *9*, 303−345.
(36) Israelachvili, J. N. *Intermolecular and Surface Forces*; Academic Press: London, 1992.
(37) Lyklema, J. *An Introduction to Colloid and Interface Science*; Academic Press: London, 1995; Vol 2.
(38) Hartley, P. G.; Larson, I.; Scales, P. J. *Langmuir* **1997**, *136*, 22207−2214.
(39) Considine, R.; Drummond, C. J. *Langmuir* **2001**, *17*, 7777−7783.
(40) Laibinis, P. E.; Nuzzo, R. G.; Whitesides, G. M. *J. Phys. Chem*. **1992**, *96*, 5097−5105.
(41) Folkers, J. P.; Laibinis, P. E.; Whitesides, G. M. *Langmuir* **1992**, *8*, 1330−1341.
(42) Atre, S. V.; Liedberg, B.; Allara, D. L. *Langmuir* **1995**, *11*, 3882−3893.
(43) Shevade, A. V.; Zhou, J.; Zin, M. T.; Jiang, S. Y. *Langmuir* **2001**, *17*, 7566−7572.
(44) Imabayashi, S.; Gon, S. N.; Sasaki, T.; Hobara, D.; Kakiuchi, T. *Langmuir* **1998**, *14*, 2348−2351.
(45) Kakiuchi, T.; Iida, M.; Gon, S. N.; Hobara, D.; Imabayashi, S.; Niki, K.; *Langmuir* **2001**, *17*, 1599−1603.
(46) Beake, B. D.; Leggett, G. J. *Phys. Chem. Chem. Phys*. **1999**, *1*, 3345−3350.
(47) Stranick, S. J.; Parikh, A. N.; Tao, Y. T.; Allara, D. L.; Weiss, P. S. *J. Phys. Chem*. **1994**, *98*, 7636−7646.
(48) Stranick, S. J.; Atre, S. V.; Parikh, A. N.; Wood, M. C.; Allara, D. L.; Winograd, N.; Weiss, P. S. *Nanotechnology* **1996**, *7*, 438−442.
(49) Bertilsson, L.; Liedberg, B. *Langmuir* **1993**, *9*, 141−149.
(50) Hutt, D. A.; Leggett, G. J. *Langmuir* **1997**, *13*, 2740−2748.
(51) Ulman, A.; Evans, S. D.; Shnidman, Y.; Sharma, R.; Eilers, J. E. *Adv. Colloid Interface Sci*. **1992**, *39*, 175−225.
(52) Yaroshczuk, A. E.; Ribitsch, V. *Langmuir* **2002**, *18*, 2036−2038.
(53) König, U.; Nitschke, M.; Menning, A.; Sperling, C.; Simon, F.; Arnhold, Ch.; Werner, C.; Jacobasch, H. J. *Surf. Coat. Technol.* **1999**, *116*−*119*, 1011−1015. (b) König, U.; Nitschke, M.; Menning, A.; Eberth, G.; Pilz, M.; Arnhold, Ch.; Simon, F.; Adam, G.; Werner, C. *Colloids Surf. B* **2002**, *24*, 63−71.
(54) Schmidt, U.; Zschoche, St.; Werner, C. *J. Appl. Polym. Sci.* **2003**, *87*, 1255−1266.
(55) Weisbecker, C. S.; Merritt, M. V.; Whitesides, G. M. *Langmuir* **1996**, *12*, 3763−3772. (b) Mayya, K. S.; Patil, V.; Sastry, M. *Langmuir* **1997**, *13*, 3944−3947.
(56) Dicke, C.; Hähner, G. *J. Am. Chem. Soc.* **2002**, *105*, 12619−12625.
(57) Ederth, T.; Tamada, K.; Claesson, P. M.; Valiokas, R.; Colorado, J., Jr.; Graupe, M.; Shmakova, O. E.; Lee, T. R. *Colloids Surf. A* **2001**, *182*, 257−261.
(58) Dunstan, D. E.; Saville, D. A. *J. Chem. Soc., Faraday Trans*. **1993**, *89*, 527−529.
(59) Kreuzer, H. J.; Wang, E. L. C.; Grunze, M. *J. Am. Chem. Soc*. **2003**, *125*, 8384−8389.
(60) Usui, S.; Healy, T. W. *J. Colloid Interface Sci*. **2001**, *240*, 127−132.
(61) Karraker, K. A.; Radke, C. J. *Adv. Colloid Interface Sci*. **2002**, *96*, 231−264.
(62) Scatena, L. F.; Richmond, G. L. *J. Phys. Chem. B* **2001**, *105*, 11240−11250. (b) Richmond, G. L. *Chem. Rev.* **2002**, *102*, 2693−2724.
(63) Aoki, K.; Kakiuchi, T. *J. Electroanal. Chem.* **1999**, *478*, 101−107.
(64) Borkovec, M. *Langmuir* **1997**, *13*, 2608−2613.
(65) Currie, E. P. K.; Sieval, A. B.; Avena, M.; Zuilhof, E. J. R.; Sudhölter, E. J. R.; Cohen Stuart, M. A. *Langmuir* **1999**, *15*, 7116−7118.
(66) Ederth, T.; Claesson, P. E. *J. Colloid Interface Sci.* **2000**, *229*, 123−128.
(67) Helm, C. A.; Laxhuber, L.; Lösche, M.; Möhwald, H. *Coll. Polym. Sci*. **1986**, *264*, 46−55.
(68) McLaughlin, S.; Mulrine, S.; Gresalfi, T.; Vaio, G.; McLaughlin, A. *J. Gen. Physiol*. **1981**, *77*, 445−473.
(69) Lochhead, M. J.; Letellier, S. R.; Vogel, V. *J. Phys. Chem. B* **1997**, *101*, 10821−10827.